Supporting information

Geometric Modulation of Induced Plasmonic Circular Dichroism in Nanoparticle Assemblies Based on Backaction and Field Enhancement

Zhi Yong Bao,[ab] Jiyan Dai,[a] Qiang Zhang,[a] Kwun Hei Ho,[a] Siqi Li,[a] Chan Cheuk Ho,[a] Wei Zhang,[c]* Dang Yuan Lei*[ad]

[a] *Department of Applied Physics, The Hong Kong Polytechnic University, Hong Kong, China*
[b] *School of Materials Science and Engineering, Hefei University of Technology, Hefei, China*
[c] *Institute of Applied Physics and Computational Mathematics, P. O. Box 8009(28), Beijing 100088, China*
[d] *Shenzhen Research Institute, The Hong Kong Polytechnic University, Shenzhen, China*

E-mail: *zhang_wei@iapcm.ac.cn
*dangyuan.lei@polyu.edu.hk

Table of contents

Fig. S8. The time-dependent LSP and CD spectra changes in the ETE assembly process.

Fig. S9. (a, b) Absorption and CD spectra of pristine CSNCs and L-cysteine assembled CSNCs under different CTAB concentrations (red curve: 200 μM and blue curve: 1 μM). (c, d) TEM images of CSNCs-200 μM and CSNCs-1 μM samples, respectively.

Fig. S10 Representative TEM and high-resolution images of L-cysteine assembled core-shell nanocrystals (aspect ratio ~3.5) with ETE (a) and SBS (b) patterns.

Fig. S11 UV-Vis (a) and CD (b) spectra of L-cysteine assembled Au nanorods with ETE and SBS patterns in comparison with pristine Au nanorods.

Fig. S12 Comparison of interparticle distances between assembled (a, b) Au@Ag CSNCs and (c,d) Au nanorods. (e,f) Proposed molecular arrangement differences of capped CTAB on the surfaces of Ag and Au.

Fig. S13 UV-Vis (a) and CD (b) spectra of L-cysteine assembled Ag nanorods with ETE and SBS patterns in comparison with pristine Ag nanorods.

Table S1 Calculated g-factors for L/D-cysteine assembled Au@Ag core-shell nanocrystals (aspect ratio ~3.8) under varied CTAB concentration.

Table S2 Calculated g-factors for L/D-cysteine assembled Au@Ag core-shell nanocrystals (aspect ratio ~3.5) with ETE and SBS assemblies.

Table S3 Calculated g-factors for L/D-cysteine assembled Au@Ag core-shell nanocrystals (aspect ratio ~3.2) with ETE and SBS assemblies.

Materials and Experiment Characterization

Materials

Chemicals: cetyltrimethylammonium bromide (CTAB), tetrachloroauric (III) acid ($HAuCl_4$), cetyltrimethylammonium chloride (CTAC), silver nitrate ($AgNO_3$), ascorbic acid (AA), trisodium citrate, sodium borohydride, L-cysteine, D-cysteine, and DL-cysteine were purchased from Sigma. All chemicals were used without further purification. Ultrapure water was used for all experiments.

Instrument and characterization

The CD spectra of all samples were measured with a commercially available CD spectrometer (JASCO, J-810). The extinction spectra of the samples were obtained with a UV-Vis spectrometer (Shimadzu Scientific Instruments, UV2550). The Raman spectra of the samples were recorded by using a commercial Raman spectrometer (HORIBA HR800) at excitation laser wavelength 488 nm (~2 μm beam diameter and 0.1 mW output power) and signal integration time of 1 sec. Each as-prepared nanostructure solution was drop-cast on a TEM grid to perform morphological

characterizations (JEM2100F TEM system operating at 200 kV).

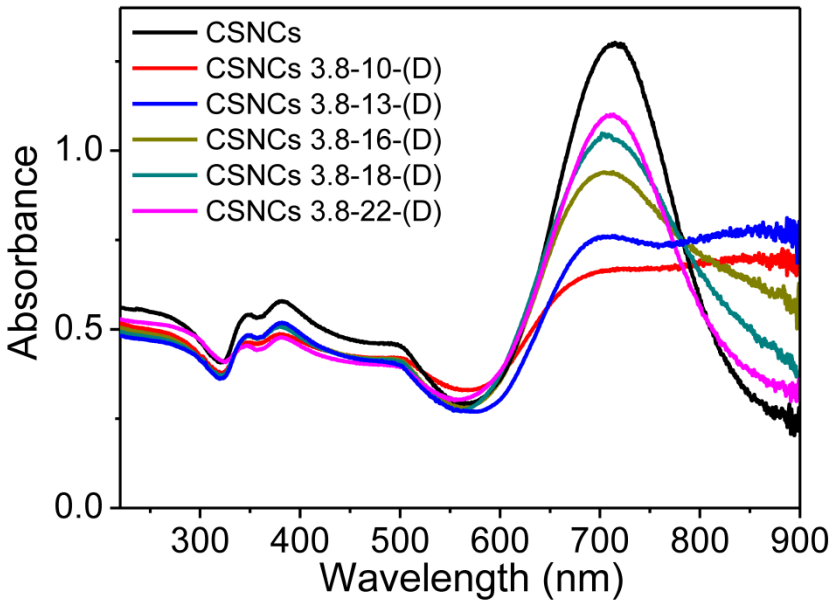

Fig. S1. Absorption spectra of D-cysteine assembled Au@Ag core-shell nanocrystals under different CTAB concentrations.

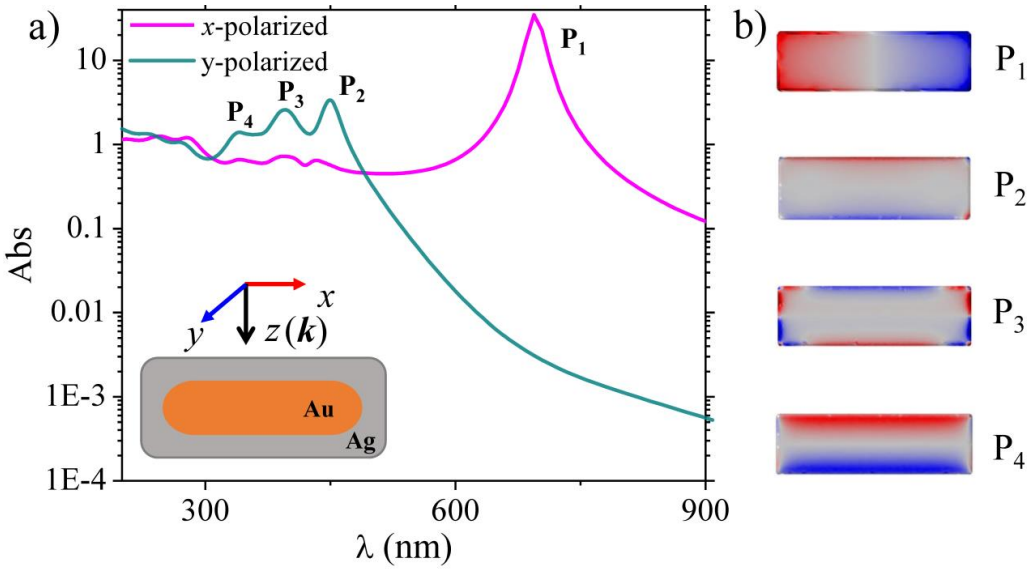

Fig. S2. (a) The simulated absorption cross sections and (b) surface charge distributions of single Au@Ag CSNC.

We numerically investigate the plasmon modes of the single Au@Ag CSNC and assembled CSNC samples *via* the commercial full wave simulation software COMSOL Multiphysics. In the simulation, the geometry parameters are set according to the measured TEM results. To avoid singularities caused by the sharp features in simulation, all the edges of the cuboid shell are 1 nm filleted. The CSNCs are dispersed in water ($n_{\text{water}} \approx 1.33$) and the permittivity of gold and silver are taken from empirical data. For simplicity, we consider that the single CSNC and assemblies are excited by normally (with respect to the long axis) incident plan waves with two orthogonal polarization directions, i.e. parallel (x-direction) and perpendicular (y-direction) respect to long axis of the nanorod. The calculated absorption cross sections of the CSNC monomer, L-coupled and T-coupled dimers are shown in Fig. S2 and Fig. S3. Firstly, from Fig. S2 (for single CSNC) it can be concluded that four absorption peaks, P_1 (695 nm), P_2 (449 nm), P_3 (395 nm) and P_4 (339 nm) correspond to longitudinal dipole, transverse dipole, octupole and multipole LSPR modes, respectively.[1]

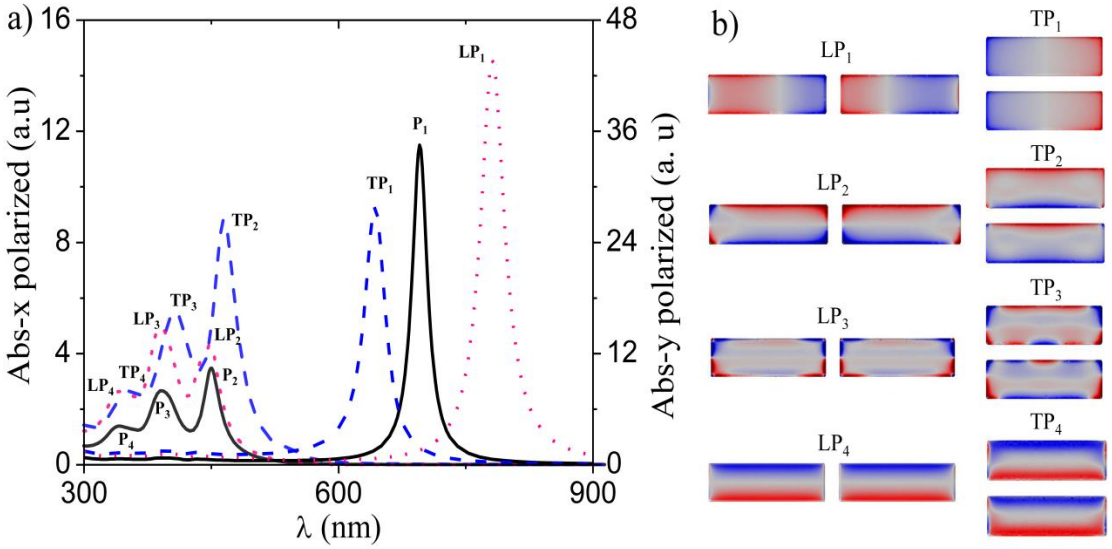

Fig. S3. (a) The simulated absorption cross sections and (b) surface charge distributions of end-to-end and side-by-side assembled Au@Ag CSNC dimer.

To simplify the calculated mode, we choose two assembled CSNCs as the calculated model. When the CSNCs are assembled to L-coupled and T-coupled dimers, (see Fig. S3), the plasmon modes (P_1~P_4) of the monomer will couple and form new plasmon modes. Similar to the monomer, we label the four new modes of the L-coupled (T-coupled) as LP_1 (TP_1), LP_2 (TP_2), LP_3 (TP_3), and LP_4 (TP_4) from the long wavelength to the short wavelength, respectively. The corresponding absorption cross sections and charge distributions are given in Fig. S3. Based on plasmon hybridization theory, the absorption wavelength of the hybridized modes depends on the coupling configuration and the excitation polarization. For example, when the excitation polarization is parallel to the coupling direction, the hybridized mode would redshifts. In case of the L-coupled dimer (x direction coupled) excited by the x-polarized plane wave, the hybridized mode LP_1 has longer wavelength than P_1. On the contrary, when the excitation polarization is perpendicular to the coupling direction, the hybridized wavelength would blueshift. For instance, the T-coupled dimer (y direction coupled) excited by the x-polarized plane wave, the hybridized mode TP_1 has shorter wavelength than that of P_1. The calculation results are consistent well with the experimental measurements.

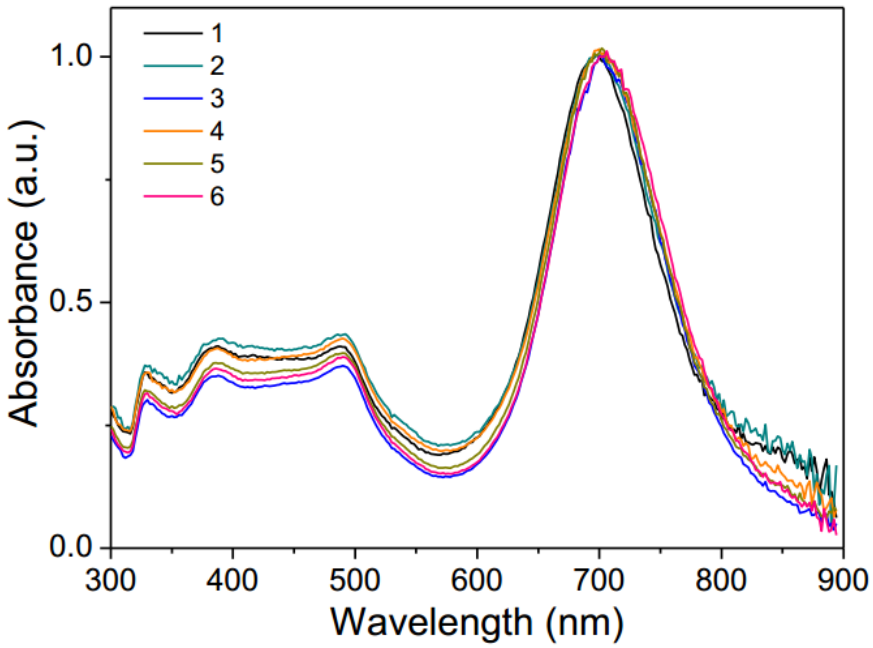

Fig. S4. The extinction spectra of CSNCs at various concentration of CTAB. 1-7 represents the CTAB increases.

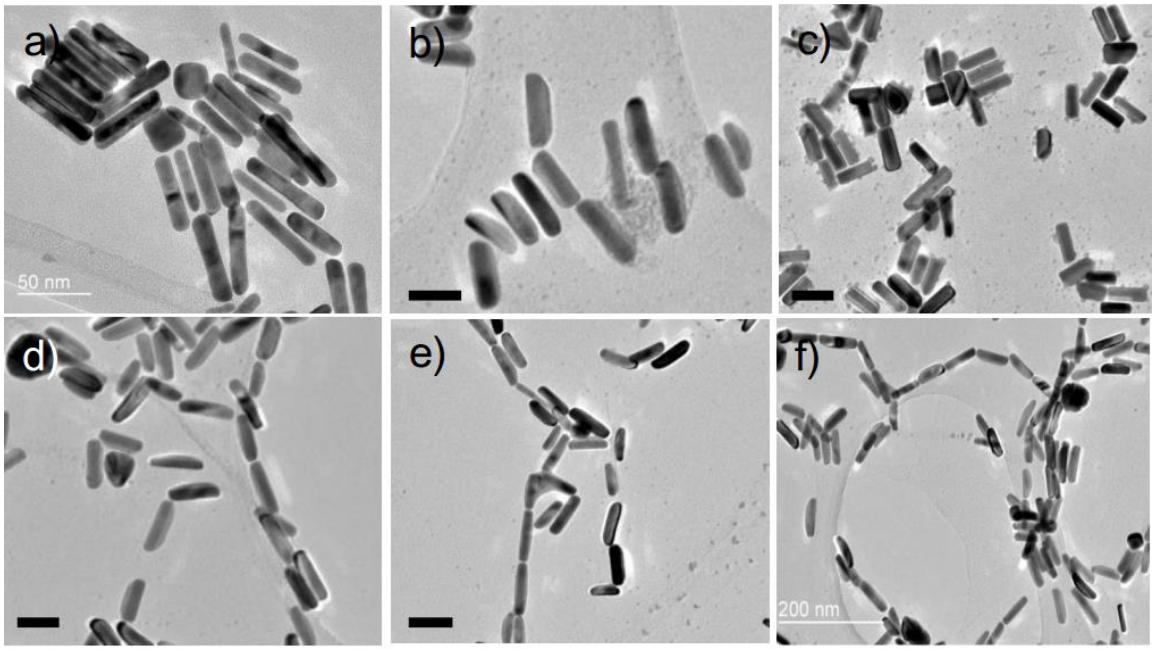

Fig. S5 Representative TEM images of SBS patterns (a), (b) and (c); ETE patterns (d), (e) and (f). The scale bar is 50 nm.

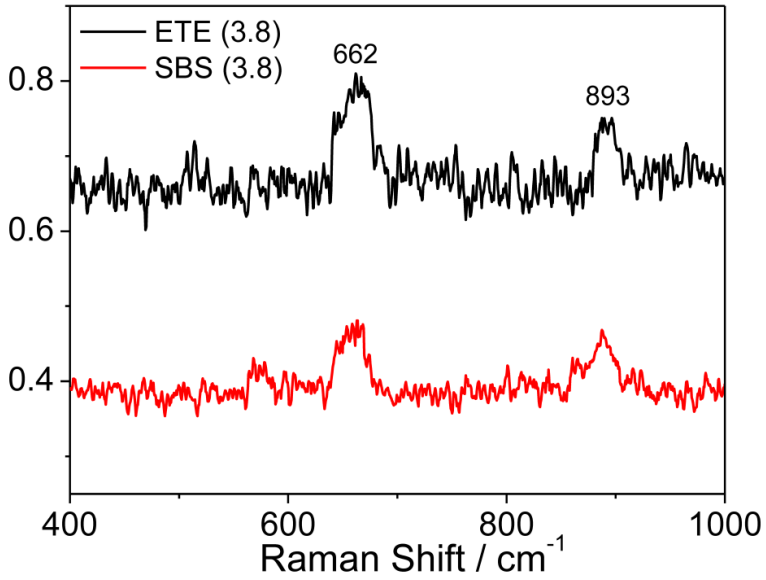

Fig. S6. SERS spectra of L-cysteine assembled ETE (black curve) and SBS (red curve) Au@Ag core-shell nanocrystals with aspect ratio of ~3.8. The peak at 662 cm^{-1} stands for the ν(C-S) mode, while the peak at 893 cm^{-1} represents the $\beta(C_\alpha COO) + \nu(C_\alpha COO)$ mode.

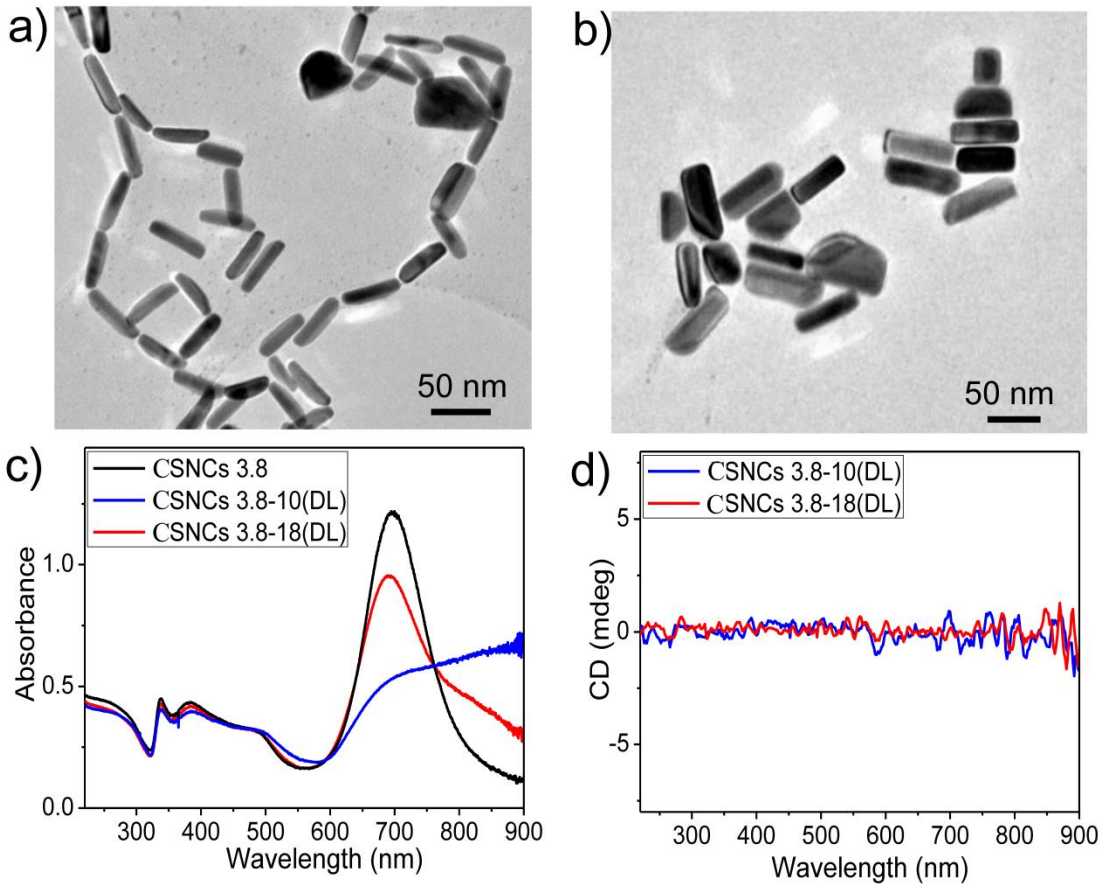

Fig. S7. Morphology and optical characterizations of DL-cysteine assembled Au@Ag core-shell nanocrystals (aspect ratio ~3.8) with ETE (a & c) and SBS (b & d) patterns.

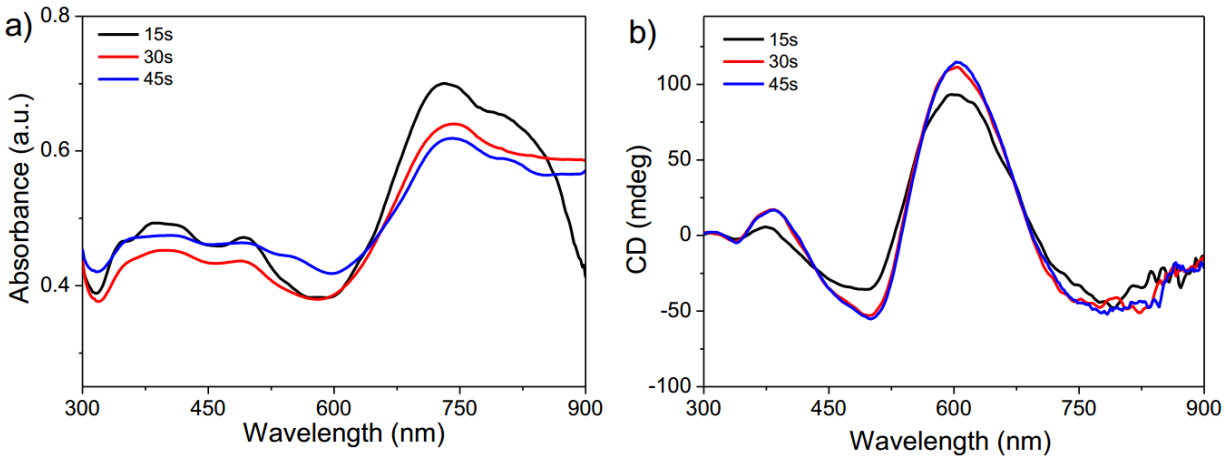

Fig. S8. The time-dependent LSP and CD spectra changes in the ETE assembly process.

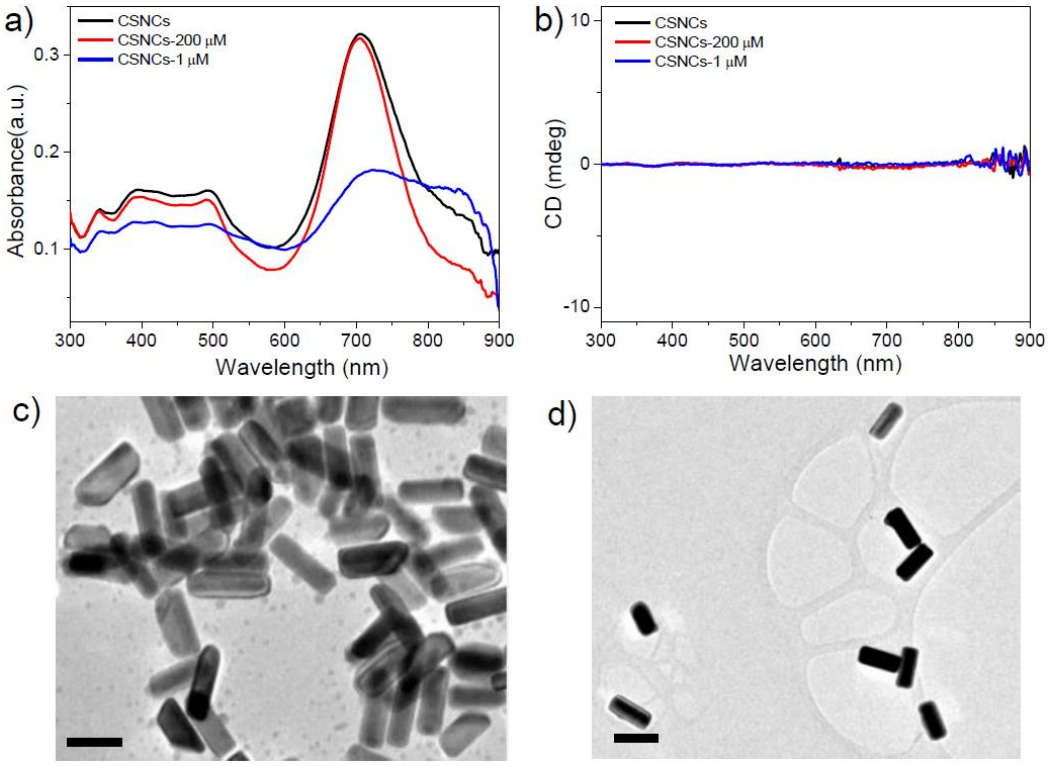

Fig. S9. (a, b) Absorption and CD spectra of pristine CSNCs and L-cysteine assembled CSNCs under different CTAB concentrations (red curve: 200 μM and blue curve: 1 μM). (c, d) TEM images of CSNCs-200 μM and CSNCs-1 μM samples, respectively.

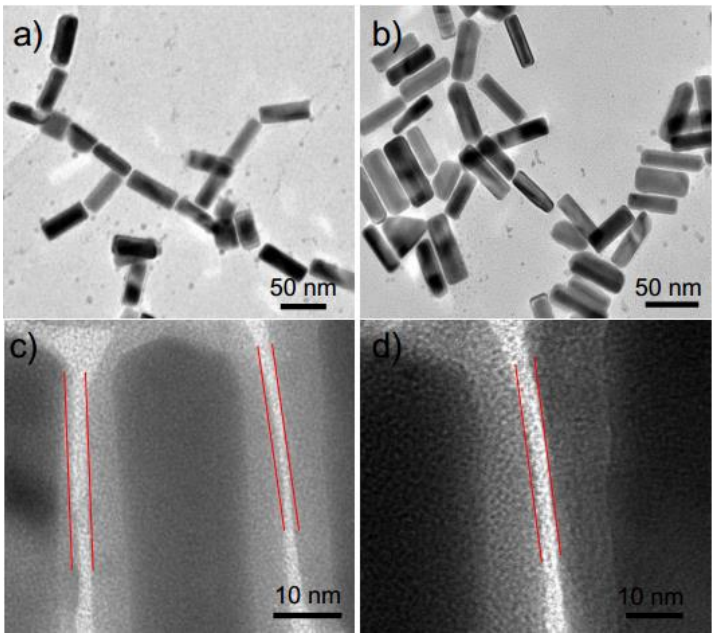

Fig. S10. Representative TEM and high-resolution TEM images of L-cysteine assembled core-shell nanocrystals (aspect ratio ~3.5) with ETE (a) and SBS (b) patterns. (c & d) clearly reveal the interparticle distance between assembled adjacent nanocrystals is ~3-4.5 nm.

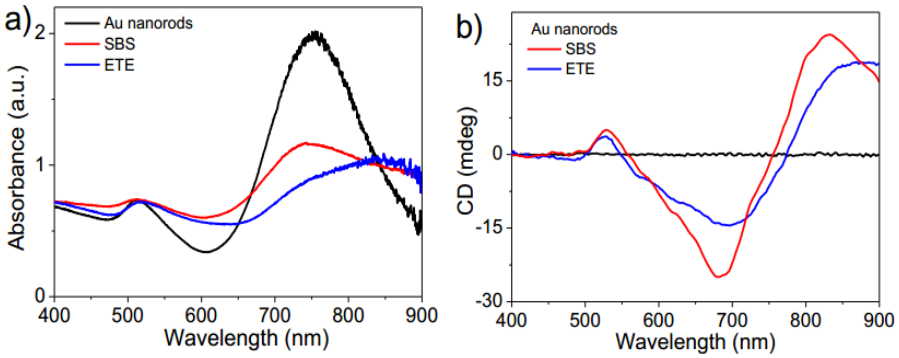

Au nanorods		CD peak ($\times10^{-3}$)	CD Peak ($\times10^{-3}$)
		510 nm	685 nm
g-factor	ETE	**0.26**	**-0.55**
	SBS	**0.33**	**-0.86**

Fig. S11. UV-Vis (a) and CD (b) spectra of L-cysteine assembled Au nanorods with ETE and SBS patterns in comparison with pristine Au nanorods. The lower panel shows the calculated g-factors for two different assembly modes.

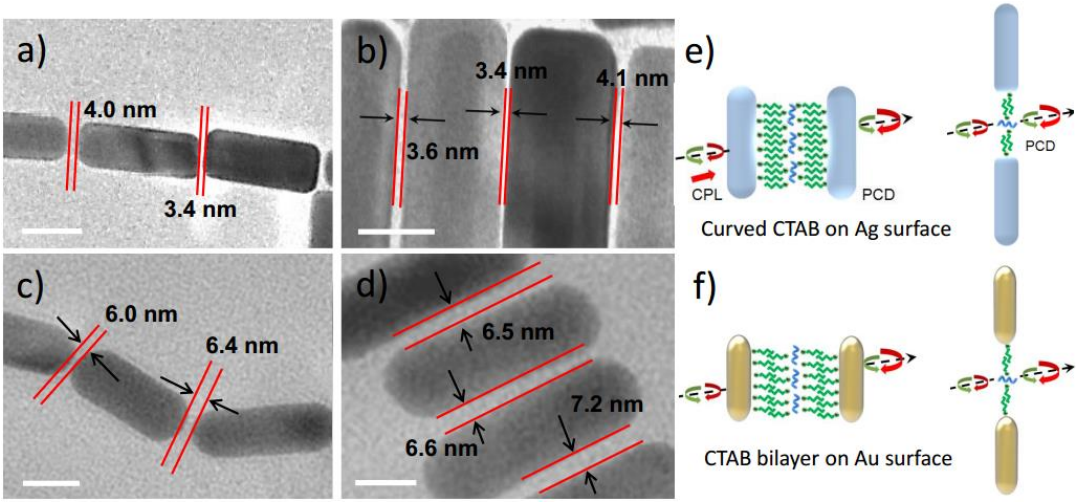

Fig. S12. Comparison of interparticle distances between assembled (a, b) Au@Ag CSNCs and (c,d) Au nanorods. It can be observed that the measured interparticle distances of Au@Ag-Au@Ag and Au-Au are ~3-4.5 and 6-7.5 nm, respectively. The distance difference is ~3 nm, just the length of two cysteine molecules, illustrating the curved CTAB bilayer on the Ag surface. (e) and (f) propose the molecular arrangement differences of capped CTAB on the surface of Ag (light blue) and Au (yellow). The green and blue curved lines represent CTAB and cysteine molecules, respectively.

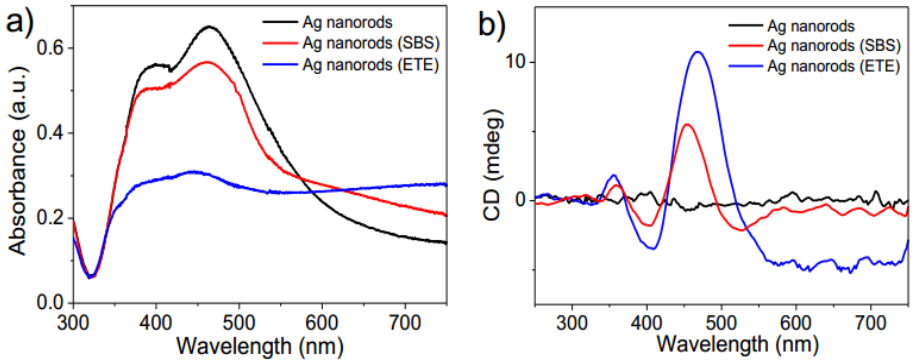

Ag nanorods		CD peak ($\times 10^{-3}$)		CD Peak($\times 10^{-3}$)
		355 nm	407 nm	450 nm
g-factor	SBS	**0.09**	**-0.11**	**0.32**
	ETE	**0.23**	**-0.36**	**1.11**

Fig. S13. UV-Vis (a) and CD (b) spectra of L-cysteine assembled Ag nanorods with ETE and SBS patterns in comparison with pristine Ag nanorods. The lower panel shows the calculated g-factors for two different assembly modes.

Anisotropic Factors (AF) of L/D-Cys-Assembled Au@Ag CSNCs

Au@Ag CSNC3.8-L		LSPR CD peak(λ/nm) (×10^{-3})			CD Peak(×10^{-3})
		334	383	497	602
g-factor ETE	10ul	**-0.37**	**1.01**	**-4.72**	**14.45**
	13ul	-0.29	0.71	-4.13	10.98
SBS	16ul	**-0.27**	**0.62**	**-2.76**	**8.97**
	18ul	-0.26	0.29	-1.21	3.63
	22ul	-0.24	0.27	-0.84	1.94
Au@Ag CSNC3.8-D		LSPR CD peak(λ/nm) (×10^{-3})			CD Peak (×10^{-3})
		336	374	497	611
g-factor ETE	10ul	**0.34**	**-0.65**	**2.95**	**-11.7**
	13ul	0.32	-0.44	1.67	-10.02
SBS	16ul	**0.29**	**-0.46**	**1.68**	**-6.43**
	18ul	0.27	-0.41	0.96	-3.91
	22ul	0.25	-0.34	0.24	-1.75

Table S1. Calculated g-factors for the L/D-cysteine assembled Au@Ag core-shell nanocrystals (aspect ratio ~3.8) under varied CTAB concentration.

Anisotropic Factors (AF) of L/D-Cys-Assembled Au@Ag CSNCs

Au@Ag CSNC3.5-L		LSPR CD peak(λ/nm) (×10^{-3})			CD Peak(×10^{-3})
		350	400	490	612
g-factor	SBS	**-0.26**	**0.19**	**-1.04**	**1.61**
	ETE	**-0.35**	**0.64**	**-1.64**	**4.30**
Au@Ag CSNC3.5-D		LSPR CD peak(λ/nm) (×10^{-3})			CD Peak (×10^{-3})
		349	401	485	606
g-factor	SBS	**0.12**	**-0.12**	**0.42**	**-0.98**
	ETE	**0.31**	**-0.40**	**0.90**	**-3.82**

Table S2. Calculated g-factors for the L/D-cysteine assembled Au@Ag core-shell nanocrystals (aspect ratio ~3.5) with ETE and SBS assemblies.

Anisotropic Factors (AF) of L/D-Cys-Assembled Au@Ag CSNCs

Au@Ag CSNC3.2-L		LSPR CD peak(λ/nm) ($\times10^{-3}$)			CD Peak($\times10^{-3}$)
		343	393	485	611
g-factor	**SBS**	**-0.07**	**0.08**	**-0.18**	**0.51**
	ETE	**-0.10**	**0.23**	**-0.37**	**1.70**
Au@Ag CSNC3.2-D		**LSPR CD peak(λ/nm) ($\times10^{-3}$)**			**CD Peak ($\times10^{-3}$)**
		340	395	479	605
g-factor	SBS	**0.07**	**-0.09**	**0.22**	**-0.41**
	ETE	**0.09**	**-0.17**	**0.45**	**-1.29**

Table S3. Calculated g-factors for the L/D-cysteine assembled Au@Ag core-shell nanocrystals (aspect ratio ~3.2) with ETE and SBS assemblies.

Anisotropy factors, g-factors, were calculated as follows: [2]

$g = \Delta\varepsilon/\varepsilon = \Omega(\text{mdeg})/(32980\times A)$

where Ω (mdeg) and *A* are the CD signal 1intensity and the UV-Vis absorption intensity of nanorod and nanocrystal solution. Take the Au@Ag CSNC3.8 for example, the maximum g-factor for L(D)-cysteine-directed ETE assembly was calculated to be 1.445×10^{-2} (1.17×10^{-2}). Individual NPs are the building blocks in the nanoassemblies. Based on plasmon hybridization theory, the absorption wavelength of the hybridized modes (nanoassemblies) depends on the coupling configuration and the excitation polarization. For example, in the ETE pattern, when the excitation polarization is parallel to the coupling direction, the hybridized mode would redshifts. In case of SBS assembly, when the excitation polarization is perpendicular to the coupling direction, the hybridized wavelength would blueshift. While the g-factors in nanoassemblies are much larger than that in individual NPs because the former has stronger coupling and near field enhancement.

References:

1 R. B. Jiang, H. J. Chen, L. Shao, Q. Li, J. F. Wang, *Adv. Mater.*, 2012, **24**, OP200-OP207.

2 Y. Zhao, L. Xu, W. Ma, L. Wang, H. Kuang, C. Xu and N. A. Kotov, *Nano Lett.*, 2014, **14**, 3908-3913.